Result from the First Science Run of the ZEPLIN-III Dark Matter Search Experiment

V. N. Lebedenko*,[1] H. M. Araújo,[1,2] E. J. Barnes,[3] A. Bewick,[1] R. Cashmore,[4] V. Chepel,[5] D. Davidge,[1] J. Dawson,[1] T. Durkin,[2] B. Edwards,[1,2] C. Ghag,[3] V. Graffagnino,[2] M. Horn,[1] A. S. Howard,[1] A. J. Hughes,[2] W. G. Jones,[1] M. Joshi,[1] G. E. Kalmus,[2] A. G. Kovalenko,[6] A. Lindote,[5] I. Liubarsky,[1] M. I. Lopes,[5] R. Lüscher,[2] P. Majewski,[2] A. StJ. Murphy,[3] F. Neves,[5,1] J. Pinto da Cunha,[5] R. Preece,[2] J. J. Quenby,[1] P. R. Scovell,[3] C. Silva,[5] V. N. Solovov,[5] N. J. T. Smith,[2] P. F. Smith,[2] V. N. Stekhanov,[6] T. J. Sumner†,[1] C. Thorne,[1] and R. J. Walker[1]

[1]*Blackett Laboratory, Imperial College London, UK*
[2]*Particle Physics Department, Rutherford Appleton Laboratory, Chilton, UK*
[3]*School of Physics and Astronomy, University of Edinburgh, UK*
[4]*Brasenose College, University of Oxford, UK*
[5]*LIP–Coimbra & Department of Physics of the University of Coimbra, Portugal*
[6]*Institute for Theoretical and Experimental Physics, Moscow, Russia*

(Dated: December 8, 2008)

The ZEPLIN-III experiment in the Palmer Underground Laboratory at Boulby uses a 12 kg two-phase xenon time projection chamber to search for the weakly interacting massive particles (WIMPs) that may account for the dark matter of our Galaxy. The detector measures both scintillation and ionisation produced by radiation interacting in the liquid to differentiate between the nuclear recoils expected from WIMPs and the electron recoil background signals down to ∼10 keV nuclear recoil energy. An analysis of 847 kg·days of data acquired between February 27^{th} 2008 and May 20^{th} 2008 has excluded a WIMP-nucleon elastic scattering spin-independent cross-section above 7.7×10^{-8} pb at 55 GeVc^{-2} with a 90% confidence limit.

I. INTRODUCTION

A. Motivation

Searches for weakly interacting massive particles (WIMPs) are motivated by the coming together of unification schemes, such as supersymmetry, which predict new particle species, and extensive observational evidence which demonstrates the need for additional non-baryonic gravitational mass within the Universe. That the WIMPs of supersymmetry naturally fulfill this need is remarkably persuasive. Indeed, WIMPs occur in other frameworks too. As a generic class of particle they are assumed to only interact non-gravitationally with baryonic matter via the weak interaction. Whilst this offers a mechanism for energy transfer and hence detection, it also implies rather low event rates and energy deposits: <0.1 events/day/kg and <50 keV respectively. This dictates the use of sensitive underground experiments capable of specifically identifying energy deposits due to elastic scattering of incoming particles from target nuclei. ZEPLIN-III is the latest in a progressive series of instruments designed to steadily push the sensitivity limits by exploring alternative approaches using xenon-based targets [1, 2].

*Deceased 11-May-2008
†Corresponding author; address: High Energy Physics Group, Blackett Laboratory, Imperial College London, SW7 2BW, UK. Email: t.sumner@imperial.ac.uk

B. ZEPLIN-III

ZEPLIN-III is a two-phase (liquid/gas) xenon time-projection chamber specifically designed to search for dark matter WIMPs. Its design and performance details have already been presented elsewhere [3, 4] and only a brief reminder is given here. The experiment is operating 1100 m underground. The active volume contains ∼12 kg of liquid xenon above an array of 31 2-inch diameter photomultipliers (PMTs). The PMTs employed during the first science run were ETL D730/9829Q [5], and they were used to record both the rapid scintillation signal, S1, and a delayed second signal, S2, produced by proportional electroluminescence in the gas phase above the liquid [6]. The PMT array was immersed in the liquid viewing upwards. The electric field in the target volume was defined by a cathode wire grid 36 mm below the liquid surface and an anode plate 4 mm above the surface in the gas phase. These two electrodes alone produce the drift field in the liquid and the field for extraction of the charge from the surface (3.9 kV/cm in the liquid) and the electroluminescence field in the gas (7.8 kV/cm). A fiducial volume for WIMP searches was defined by using a time window for delays between S1 and S2, which selected a depth slice within the liquid, and by 2-D position reconstruction from the PMT signals to select a radial boundary at 150 mm. This defined a fiducial volume containing 6.5 kg of xenon.

The PMT signals were digitised at 2 ns sampling over a time segment of ±18 μs either side of the trigger point. Each PMT signal was fed into two 8-bit digitisers (ACQIRIS DC265) with a ×10 gain difference between them provided by fast amplifiers (Phillips Scientific 770), to obtain both high and low sensitivity read-out covering a

wide dynamic range. The PMT array operated from a common HV supply with attenuators (Phillips Scientific 804) used to normalise their individual gains. The trigger was created from the shaped sum signal of all the PMTs. For nuclear recoil interactions the trigger was always caused by an S2 signal for energies up to 40 keVee, where keVee is an energy unit referenced to the equivalent S1 signal produced by 122 keV γ-rays from ^{57}Co. The trigger threshold was $\sim$11 ionisation electrons and this corresponded to $\sim$0.2 keVee for electron recoils. For nuclear recoils see Section III D 2. This threshold was set on S2 to avoid excessive triggers from single electron emission events and from electron and nuclear recoils whose primaries would otherwise have been undetectable as they fall below the S1 detection threshold.

The xenon target was contained within a vessel itself located within a vacuum jacket both made from low-background oxygen-free copper. Cooling was provided by a 40 litre liquid nitrogen reservoir, also made from copper, inside the vacuum jacket. Thermal stability to $<$0.5 ^{o}C was achieved over the entire run by controlling the flow of cold nitrogen boil-off gas through the base-flange of the xenon vessel. Pressure stability to 2% was maintained. The ZEPLIN-III detector was completely surrounded by a shield of 30 cm thick polypropylene and 20 cm thick lead, giving 10^5 attenuation factors for both γ-rays and neutrons from the cavern walls. Dedicated access through the shield was provided for the radioactive calibration source delivery, instrument levelling screws and pipework to the external gas purification system.

C. Science Data

WIMP-search data were collected over 83 days of continuous operation in the Boulby Laboratory starting on 27^{th} February 2008. An 84% live time was achieved during the science run and some 847 kg·days of raw data were collected from the 12 kg target volume. ^{57}Co calibration measurements were made every day. Nuclear recoil calibrations were made with an AmBe neutron source at the beginning and end of the 83 day period (5 hrs each). A typical event, from a neutron elastic scattering interaction depositing 5 keVee in the liquid, is shown in Figure 1 as recorded through the high-sensitivity sum channel. A short Compton calibration was performed using a ^{137}Cs source at the beginning of the run with a much longer run at the end (122 hrs). To begin with, 90% of the science data were retained unopened to carry out a 'blind' analysis. The remaining 10% (every 10^{th} file) were used to develop the data analysis and selection cuts, to establish the level of the electron-recoil background and to define the boundaries for the WIMP-search box and its acceptance.

Pulse-finding algorithms were used to identify signals in the 62 waveforms (independently for each PMT and for high and low sensitivity channels). These were then categorised as S1 or S2 candidates based on a pulse width parameter (charge mean arrival time, τ): scintillation pulses are much shorter ($\tau \lesssim 40$ ns) than electroluminescence pulses, with durations corresponding to the drift time across the gas gap ($\tau \sim 550$ ns). Viable S1 and S2 candidates were then subject to software thresholds ($\geq$3 channels recording signals above 1/3 photoelectron (p.e.) for S1 and a minimum area of $\sim$5 ionisation electrons for S2). Only events with one S1 and one S2 were considered for further analysis. Of particular note here, χ^2 goodness of fit indicators within the position reconstruction of both S1 and S2 were used to remove multiple-scatter events, and this was particularly effective for those with one vertex in a 'dead' region of the xenon, which would otherwise have been a troublesome background. Such 'dead' regions include the reverse-field volume between the cathode wire and the PMT grid wire [4] and the thin (0.5 mm) layer of xenon surrounding the PMT bodies. Double-Compton interactions with at least one vertex in these regions, referred to as 'multiple-scintillation single-ionisation' (MSSI) events, fulfil the previous selection criteria since there is no S2 pulse from the dead region and the coincident scintillation pulses are added together in a single S1. Unfortunately, perfecting this selection eventually required use of the full dataset as will be described in more detail below and the final analysis result is no longer 'blind'.

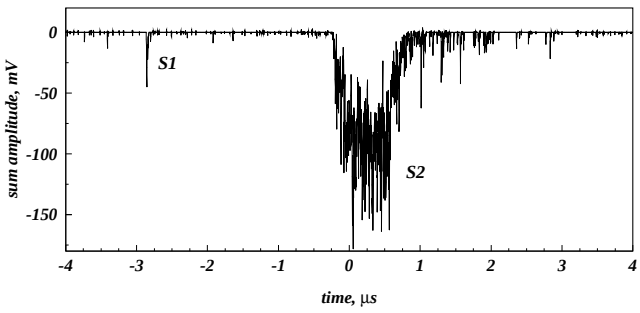

FIG. 1: Segment of the high-sensitivity summed waveform for a 5 keVee neutron elastic scatter, showing a small primary pulse (S1) preceding a large secondary pulse (S2). Some PMT after-pulsing and, possibly, single electron emission can be seen following S2. Note that only excursions >3 *rms* on individual channels are added into the summed waveform. See later text for more detailed discussion of some of these points.

II. CALIBRATION

A. Scintillation Response and Position Reconstruction

An external ^{57}Co source was inserted through the shield and located above the instrument every day. The dominant 122 keV γ-rays have a photoelectric absorption length of 3.3 mm in liquid Xe, and hence provided good standard calibration candles from interactions close to

the liquid surface. A typical ^{57}Co spectrum is shown in Figure 2. The S1 signal channel exhibited a light detection efficiency at our operating field (3.9 kV/cm) of L_y =1.8 p.e./keVee, decreasing from 5.0 p.e./keV on application of the electric field. The 122 keV interactions were used for a number of purposes to properly calibrate the instrument. Using S2 pulses, an iterative procedure, whereby a common cylindrical response profile was fitted to each channel, was used to normalise the measured response from each PMT (i.e. 'flat-field' the array). Position reconstruction in the horizontal plane was then achieved by using the converged response profiles in a simultaneous least-squares minimisation to all channels [7]. This method complements the Monte Carlo template matching procedure also being used but is less dependent on accurate iterative simulations [8]. Finally, the integrated areas of the S1 and S2 responses gave light collection correction factors as a function of radial position. Using this procedure a full-volume energy resolution of σ=5.4% at 122 keV was obtained with an energy reconstruction using a combination of the S1 and S2 responses to reflect the fact that, for electron recoils, these two channels are anti-correlated at a microscopic level. The individual S1 and S2 resolutions at 122 keV are 16.3% and 8.8%, respectively. Also shown in Figure 2 is the comparison of the response to simulation. Not only are the two main ^{57}Co lines well fitted but there is also a good match to the predicted Compton feature at ∼35 keV. The excess above 150 keV is mainly due to the unsubtracted background. Figure 3 shows the radial distribution of events seen from the source. As expected most events are located towards the centre (the offset is due to an offset source position) with a radial fall-off due to the increasing thickness of copper along the line of sight.

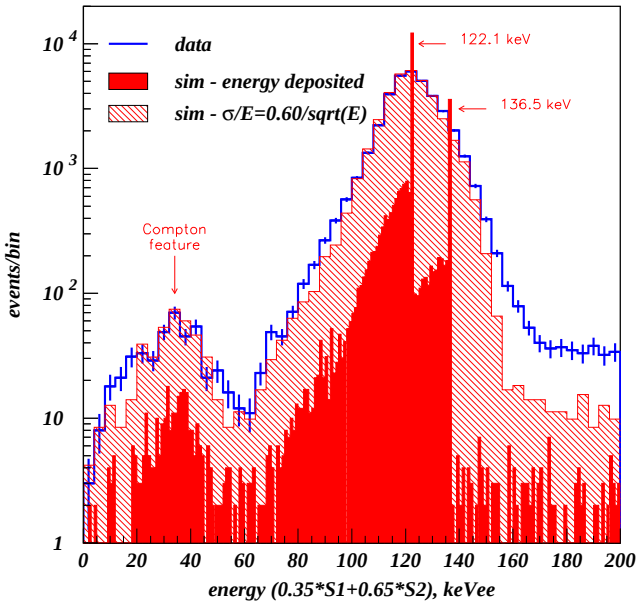

FIG. 2: Response to an external ^{57}Co γ-ray source in the combined energy channel, exploiting S1 and S2 anti-correlation. One day's experimental data are shown in blue with statistical error bars. The simulation result is indicated in red: the solid histogram shows the bare energy deposits and the shaded one shows the result of Gaussian-smearing with the energy resolution indicated in the figure.

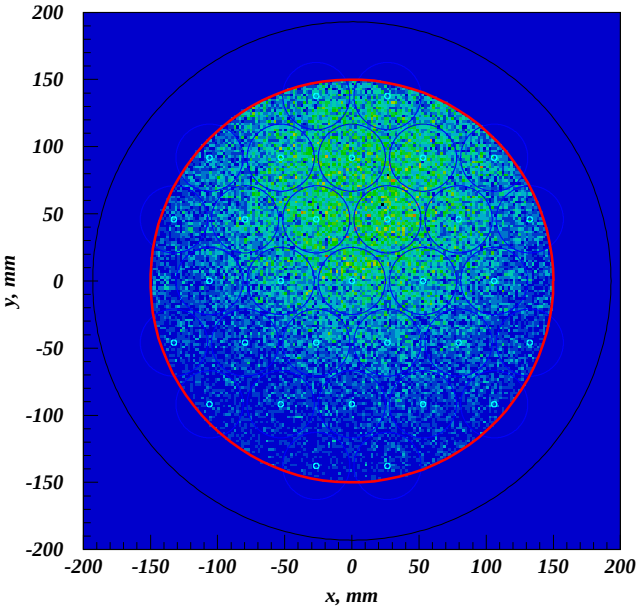

FIG. 3: Distribution in the horizontal plane of events from the ^{57}Co source. The centre is offset due to source positioning, but interaction vertices can be seen out to the edge of the fiducial volume at a radius of 150 mm (red circle). The outer circle shows the edge of the liquid xenon target. Each PMT is marked by two smaller circles (PMT centres and envelopes).

B. Stability, Electron Lifetime and Detector Tilt

The ^{57}Co daily calibrations were used to assess the evolution of other operational parameters over the entire run: i) the average light and ionisation yields, as measured by fits to the ^{57}Co S1 and S2 pulse area spectra; ii) the mean electron lifetime in the liquid, obtained from the exponential depth dependence of the ratio of the areas of the S2 and S1 signals (hereafter simply referred to as S2/S1); iii) the evolution of the long-term detector tilt due to local geological factors, as given by the polar dependence of the S2-width distribution, which probes the thickness of the gas layer. The detector tilted by less than 1 mrad over the run, which was not deemed sufficient to warrant a full correction. The scintillation mean light yield remained stable to a few percent, as did the ionisation yield, after correcting for the electron lifetime in the liquid. Remarkably, the lifetime did show an evolution during the run in the form of an improvement: from an initial value of 20 μs, achieved by initial gas-phase purification through external getters, a value of 35 μs had

been reached by the end of the run (the full drift length of the chamber is only 14 μs). There was no active recirculation used and this improvement is attributed to the clean, xenon-friendly materials used in detector construction and to the uninterrupted application of the electric fields during the entire run. As the area ratio S2/S1 is the main discriminant between nuclear and electron recoils, a depth-dependent correction must be applied to the S2 area to compensate for electron trapping by impurities. The daily ^{57}Co calibrations allowed this to be monitored throughout the science run and events were corrected individually using an historical trend profile.

C. Linearity

The linearity of the response of each channel in the array was investigated using low-energy Compton-scattered events from the ^{137}Cs source, in order to rule out hardware and software distortion for processing of small signals. Channels located a certain distance away from each interaction vertex were selected based on the expected number of S1 photons. Provided that this number is indeed small, the mean of the Poisson distribution for the number of detected photons can be quite accurately determined by counting the frequency of 'zeros', i.e. the frequency characterising the absence of any signal. This assertion is made against a sample of pure noise in the same waveform. Repeating this procedure for all channels and a range of expected signal allowed comparison of the mean S1 pulse area recorded in each trial against the expected Poisson mean, as shown in Figure 4 for the central PMT. In addition, this provides a very robust method to obtain the mean size of one photoelectron [9]. This has been calculated for every PMT within the array: the relationship is found to be linear to within the statistical accuracy of the measurement over a factor of 10 in mean pulse area, which covers the range of interest for WIMP nuclear recoil signals. The slope of the line in Figure 4 provides a measure of the mean single photoelectron (spe) response for that PMT. The spe for all the PMTs in the array has been found in this way to be in the range 47 ± 12 pVs. The spread in these values forms part of the 'flat-field' correction discussed earlier; other dominant factors are the PMT quantum efficiency and imperfect hardware equalisation.

D. Nuclear Recoil Response

The nuclear recoil response in the energy range of interest to WIMP signals has been calibrated with neutrons from an AmBe (α,n) source. The source was placed inside the polypropylene shielding above the detector but displaced to one side to reduce the interaction rate. Figure 5 shows the reconstructed event positions from the second calibration performed just after the science run had been completed. The distribution is slightly non-uniform in the x-y plane as expected.

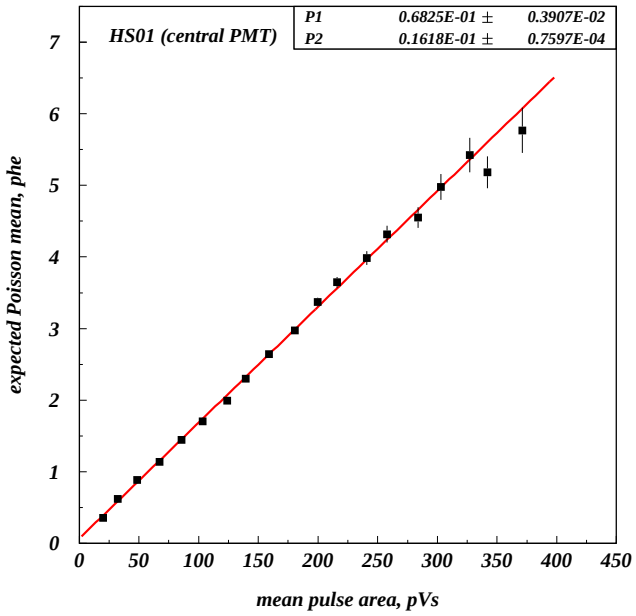

FIG. 4: Expected mean number of S1 photoelectrons as a function of the mean pulse area observed in the central channel in the array. The expected signal is the mean of the Poisson distribution obtained by counting the frequency of 'zeros', i.e. the absence of any response.

Figure 6 shows a 'scatter-plot' of $\log_{10}(S2/S1)$ as a function of energy in keVee from the AmBe calibration. The red line shows a smooth fit to the median of the elastic scatter distribution with $\pm 1\sigma$ boundaries as blue lines. To obtain these curves the data were histogramed into 1 keVee bins and fitted by log-normal distributions. Examples of the quality of the fits are shown in Figure 7. The other well defined population in Figure 6, between 40–70 keVee, is due to inelastic scattering of neutrons from ^{129}Xe nuclei and the more diffuse horizontal population is caused by associated γ-ray interactions. The elastic nuclear recoil median turns out to be very closely approximated by a power law, which is shown most effectively by replotting the figure in log-log form (Figure 8). Not only is the power-law behaviour very apparent but it can also be seen that there is less obvious flaring at lower energies than seen in other xenon experiments whose data were taken at much lower electric fields [2, 10]. Also shown are lines illustrating the approximate thresholds for S1 and S2.

E. Electron Recoil Response

The electron recoil response at low energies was established using a long duration calibration with a ^{137}Cs radioactive source. Compton scattering of the 662 keV

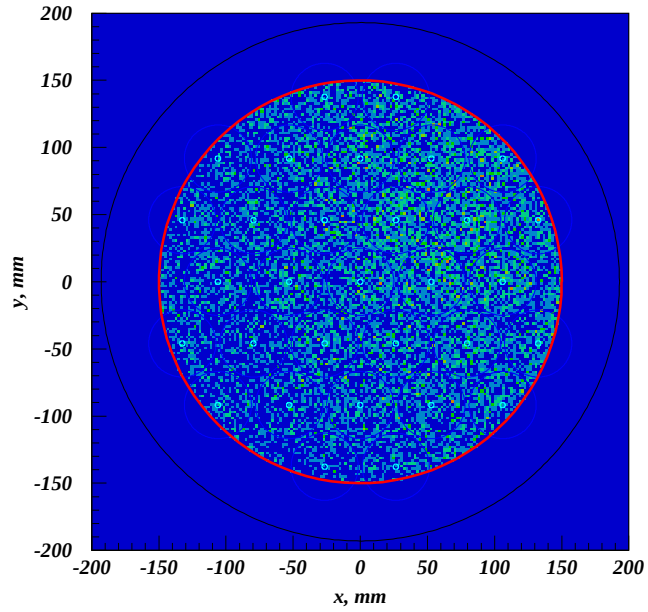

FIG. 5: Horizontal plane distribution of events from the AmBe source.

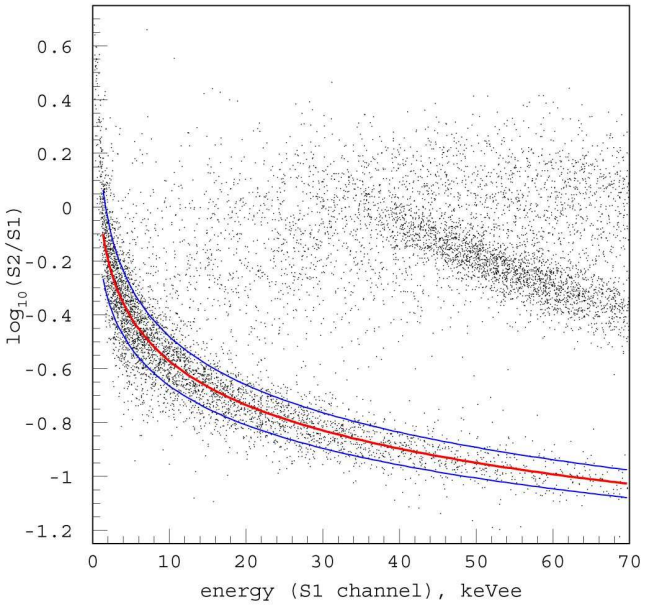

FIG. 6: Calibration of the nuclear recoil response with an AmBe neutron source, plotted as the discrimination parameter ($\log_{10}(S2/S1)$) as a function of 'electron-equivalent energy' (i.e. using the S1 channel calibrated by ^{57}Co). The lines show the trends of the mean and standard deviation of energy-binned log-normal fits to the recoil population. The distinct population above ∼40 keVee is due to inelastic neutron scattering off ^{129}Xe nuclei.

γ-rays produced a significant number of events down to $\sim$ 2 keVee but with only a small number extending far enough down in the S2/S1 parameter to reach the nuclear recoil median (Figure 9). The general behaviour of the electron recoil band is reminiscent of the XENON10 results [10, 11, 12], but with a slightly more pronounced upturn at low energy, a larger separation between electron and nuclear recoil bands and narrower distributions. The low-energy electron-recoil populations in the ^{137}Cs and the WIMP-search datasets were fitted in 1 keVee bins by a skew-Gaussian function. The fits were performed using a maximum likelihood (ML) method with a Poisson distribution as estimator for the observed data. Three of the fits are shown in Figure 7. The distribution parameters are entirely consistent bin-by-bin for the ^{137}Cs and WIMP datasets, as confirmed in Figure 9. However, the behaviour of the ^{137}Cs dataset in the low S2/S1 tails was not closely representative of the science data, with the former exhibiting significantly more outliers. This was attributed to MSSI double-Compton events.

Double-Compton events in which both vertices are within the active volume produce two primary signals which are time coincident, but separated in position, and two secondary signals which are separated in both time (delay) and position. Even if they can not be separated they are of no consequence as the combined ratio of S2/S1 will be relatively unaffected. However, if one of the vertices occurs in a position from which no secondary is possible, then the only way to identify them is through positional mismatch between S1 and S2 and a less well reconstructed position from S1 as this has two vertices. If the 'dead' vertex is very close to one of the PMT surfaces the S1 signal can also appear to be too peaked within the array. Although there were already specific software cuts designed to deal with these events, some with certain topologies were not being fully identified by our analysis at that stage. For the ^{137}Cs data this problem was most apparent in the region $\log_{10}$(S2/S1)<-0.5 and E>30 keVee but extended right down to the lowest energies. The ^{137}Cs calibration data were thus used to improve our algorithms for identifying MSSIs and the new routines were implemented after the science data had been opened. Even with the improved selection cuts it was still not possible to use the ^{137}Cs data to accurately predict the expected number of single-scatter events leaking into the nuclear recoil region as the distribution was still not fully representative of the science data, probably due to the location of the ^{137}Cs source not accurately mimicking that of the background sources. Instead the WIMP-search data themselves were used to predict the expected electron-recoil backgrounds, and this gave 11.6±3.0.

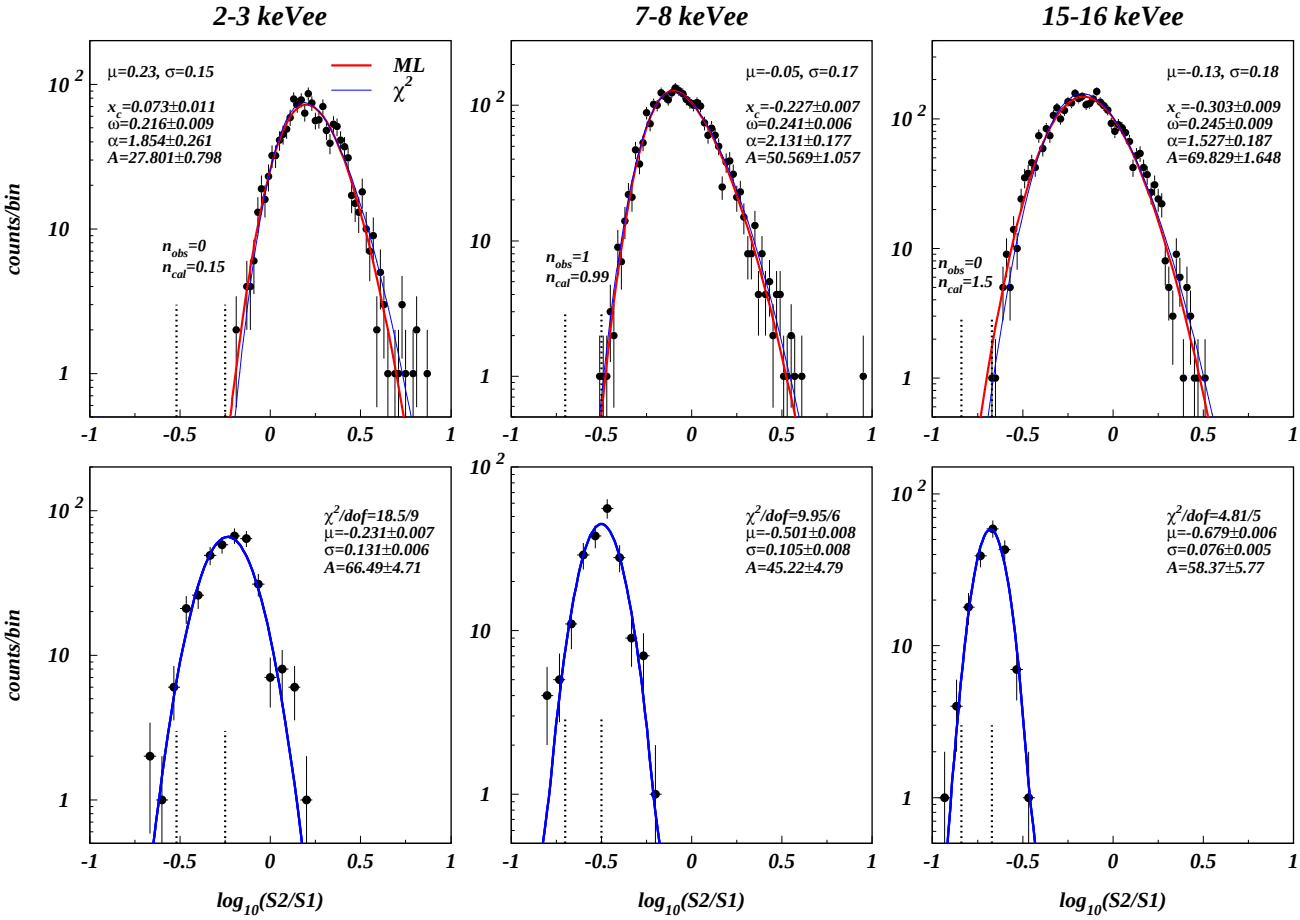

FIG. 7: Statistical fitting of the electron and nuclear recoil populations using the WIMP-search (upper panel) and AmBe datasets (lower panel). Three 1-keVee wide bins are shown: lowest, intermediate and highest energies accepted. The electron recoil population was fitted with a skew-Gaussian function using both the minimum χ^2 (thin blue line) and a maximum likelihood (ML) method (thick red line). The latter reproduced the data more accurately. Note that the entire population can be fitted in this way (all energy bins, across the entire $\log_{10}(S2/S1)$ range). The ML best fit parameters are indicated, along with the mean and standard deviation of the skew-Gaussian. The lower panels show the log-normal fits to the AmBe recoil data, which is used to define the acceptance region $[\mu–2\sigma,\mu]$, between the vertical dashed lines. The expectation of the number of electron recoils leaking into this region, n_{obs}, is compared with the predicted number, n_{cal}, from the ML fits. The total number of events predicted in the acceptance region is 11.6±3.0.

III. ANALYSIS OF THE WIMP SEARCH DATA

A. Data processing and selection

The raw data were reduced using the purpose-developed code ZE3RA (ZEPLIN-III Reduction and Analysis). The DAQ hardware records the 62 waveforms at 500 MS/s (2 ns samples) for 36 μs periods. ZE3RA finds candidate pulses in individual waveforms by searching for 3 *rms* excursions above the baseline. Subsequent waveform processing includes resolving adjacent/overlapping pulses and grouping of statistically consistent structures (e.g. scintillation tails). A statistically-motivated timing/shape coincidence analysis was then used to correlate occurrences on different channels thus allowing further pulse interpretation (e.g. clustering, identification of random coincidences, etc.) The resulting pulses were ordered by decreasing area in the high-sensitivity (HS) sum channel and the largest 10 were stored in databases for further analysis. By design, ZE3RA does not ascribe physical meaning to pulses, it rather parameterises them in terms of arrival time, width, area, amplitude, etc. An event browser allows visual scanning of events, channels or individual pulses; a batch-mode interface allows scripted reduction of large datasets.

The data structures produced by ZE3RA were analysed by a flexible code based on hbook [13]. It processed the original parameters to assign physical meaning to pulses in events according to a well defined set

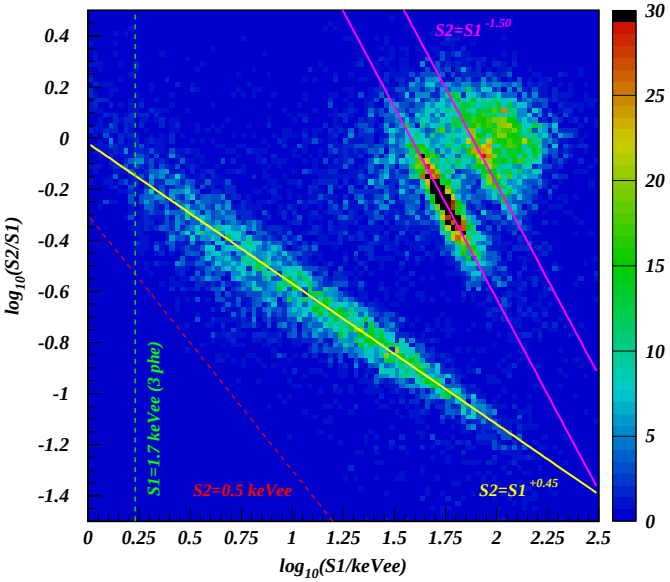

FIG. 8: Double-logarithmic plot of Fig. 6 showing the nuclear recoil population obeying the power-law trend indicated by the yellow line; the behaviour of the inelastic line from ^{129}Xe is markedly different, as this is dominated by charge recombination of the 40 keV γ-ray rather than the small nuclear recoil component of the deposited energy. Approximate thresholds for S1 (3-fold software trigger) and for S2 (hardware trigger) are also indicated.

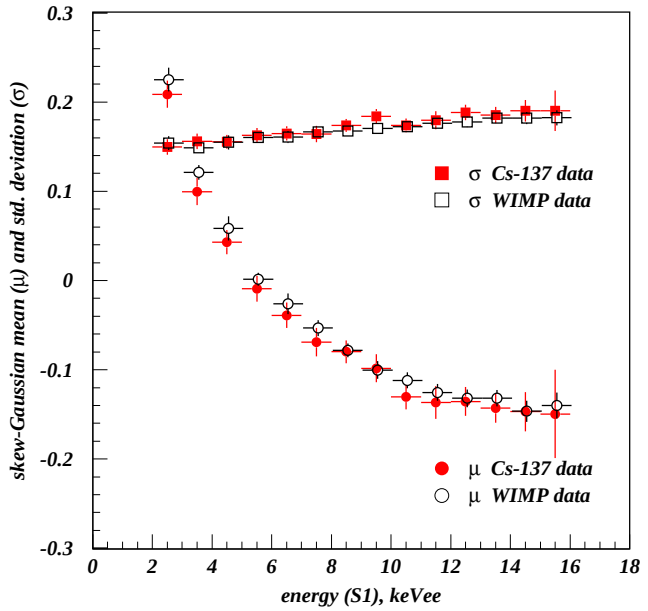

FIG. 9: Comparison of the skew-Gaussian mean and standard deviations for the ^{137}Cs and WIMP-search datasets calculated from the ML-fit parameters (the horizontal error bars indicate the bin width).

of rules (e.g. primary scintillation signals are fast and must precede wider electroluminescence signals). Only events that can represent single scatters in the two-phase target ('golden' events with one S1 and one S2) were retained. Primary (S1) pulses were found by applying an acceptance threshold of 1/3 spe to the ZE3RA pulses and also requiring a 3-fold coincidence amongst the 31 PMTs. This software threshold was nominally equivalent to an energy threshold of 1.7 keVee. Exceptions in the S1 selection were allowed for PMT after-pulses. These are signal-induced artifacts generated within the PMTs. In general they have a characteristic time delay from the optical signal, but with a wide distribution and, moreover, it varies between PMTs. As a result it is not trivial to identify after-pulsing and avoid them instead being classified as additional S1 signals, which would result in the event being wrongly rejected. Secondary (S2) pulses were required to have an integrated area corresponding to the signal expected from about 5 electrons leaving the liquid surface. This suppresses optically-induced single-electron emission [20] as well as optical feedback effects from the cathode grid, which are not part of the direct measure of the ionisation signal generated at the interaction site. Many additional parameters are derived for these, such as 3-D position information, hit-pattern descriptors, interaction energy and corrections (e.g. array flat-fielding, electron lifetime, liquid level, light collection, etc). Subsequent analysis (science exploitation) is based on PAW [14] and ROOT [15].

Trapping MSSI events effectively was a significant challenge, involving a combination of approaches: use of goodness of fit indicators in the position reconstruction algorithms, comparison of coordinates derived independently from S1 and S2, and searching for abnormal light patterns across the array.

B. The WIMP Search Box

Discrimination between nuclear and electron recoils is illustrated in Figure 10 which combines electron recoil data from ^{137}Cs and elastic nuclear recoil data from AmBe. The separation between the two populations is clear and this is used as the main way of defining the nuclear recoil search box for potential WIMP events. The selection cuts used can be categorised as follows:

1. Golden event selection (including pulse finding, S1 and S2 definition, and single scatter selection)

2. Waveform quality cuts (mild cuts mainly aimed at baseline excursions compromising pulse parameters)

3. Pulse quality cuts (mild cuts to avoid extreme outliers in parameter distributions)

4. Fiducial volume definition (drift time window and a radial limit from the S2 position reconstruction)

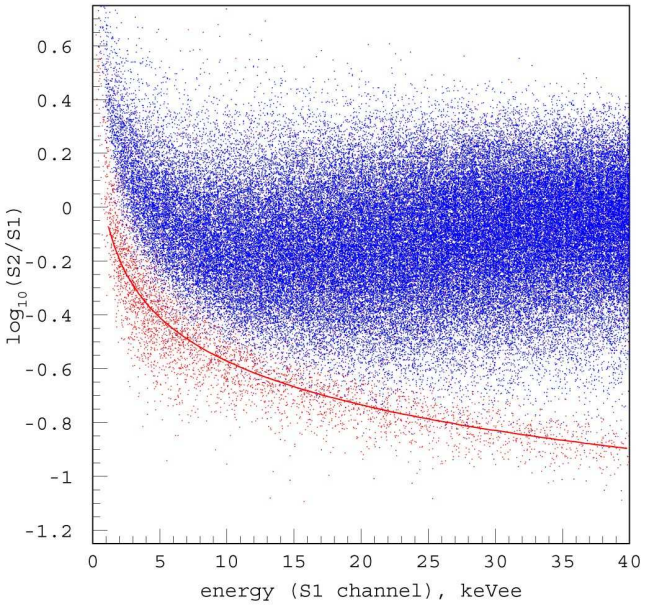

FIG. 10: Combined scatter plot of $\log_{10}(S2/S1)$ as a function of energy from the two calibration datasets, ^{137}Cs and AmBe. The upper population corresponds to low-energy Compton electrons and the narrower, lower one to nuclear recoils produced by neutron elastic scattering.

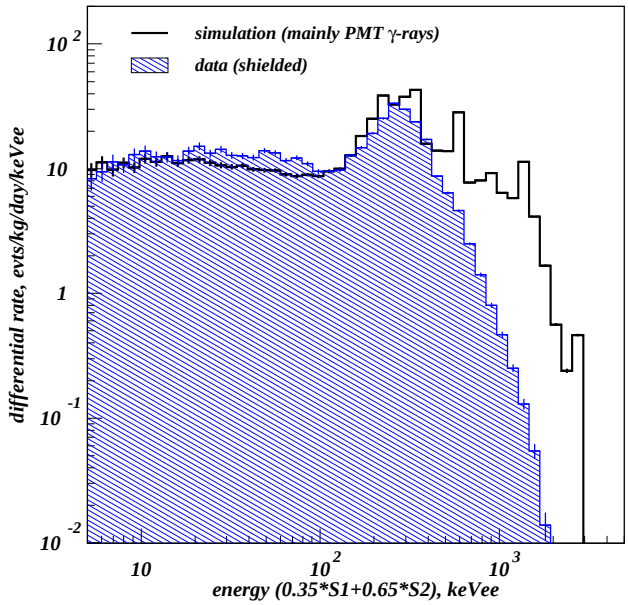

FIG. 11: Electron recoil background measured during the fully-shielded science run. The differential spectrum is shown superimposed on the Monte Carlo prediction [3] using GEANT4 [16] without rescaling. The latter includes a dominant 10.5 evts/kg/day/keVee ('dru') from the photomultipliers, γ-rays from the lead 'castle' (0.7 dru), β-particles from ^{85}Kr (0.2 dru) and γ-rays from ceramic feedthroughs (0.1 dru). The disagreement at high energies is caused by single-scatter selection in the data (but not in the simulation) and by the limited DAQ dynamic range which was optimised for the WIMP-search run.

5. Event quality cuts (strong cuts to deal with MSSI events mainly)

The fiducial definitions (4) leave a fiducial mass of 6.52 kg with a raw exposure of 453.6 kg.days. Low-energy events in the 10% data were well separated from the nuclear recoil median line down to the lowest energies. The WIMP search box boundary was thus defined as $2<E<16$ keVee and $(\mu_n-2\sigma)<\log_{10}(S2/S1)<\mu_n$, where μ_n is the energy-dependent mean of the nuclear recoils (acceptance of 47.7%). This region was defined before unblinding and was kept for the subsequent analysis. The effective total exposure within this box, after taking account of all of the efficiencies, as detailed in Table I, is 126.7 kg·days.

C. Backgrounds

Electron and nuclear recoil background predictions for ZEPLIN-III are based on a full GEANT4 [16] simulation including measured radioactive content levels for all major components. The largest contributor, by far, is the PMT array. Figure 11 shows the measured differential background spectrum together with the simulated background. The high-energy region above 300 keVee is suppressed due to dynamic range limitation.

The expected neutron background in the dataset is 1.2 ± 0.6 in the WIMP search box and this is again dominated by PMT generated events through (α,n) interactions and spontaneous fission of ^{238}U.

D. WIMP Signal Search

Figure 12 shows the final scatter plot from the complete science dataset. There are 7 events within the WIMP search box and the energy scale is shown in keVee. To assess the implications of these events the energy scale needs to be converted into keVnr, the energy dependent detector efficiency for nuclear recoils must be found and the relative likelihood of any of those 7 events being drawn from the expected WIMP distribution rather than the extended electron-recoil distribution must be calculated.

The level of discrimination apparent in Figure 12 is very high. As derived from the data themselves, the average γ-ray rejection factor is 5×10^3 between 2–16 keVee with an increase below 5 keVee. Figure 13 shows the spatial x-y distribution of all events in the 2–16 keVee energy range. Events within the WIMP search box are highlighted.

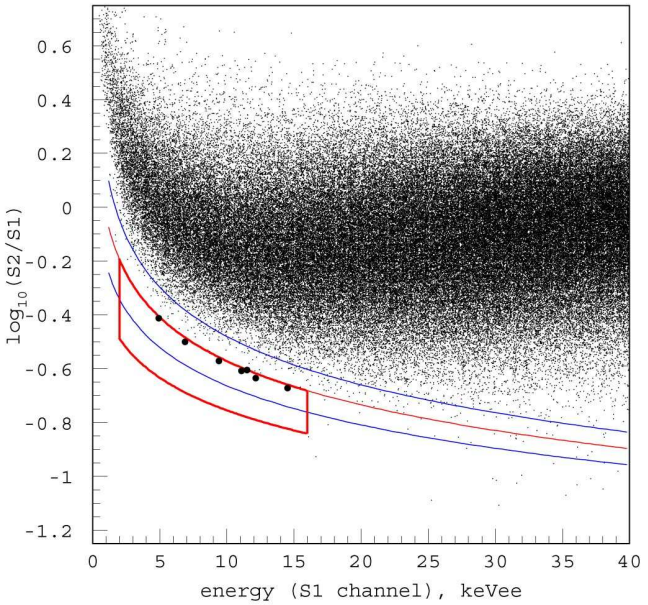

FIG. 12: Scatter plot of $\log_{10}(S2/S1)$ as a function of energy for the entire 83-day dataset of first science run. There are 7 events in the WIMP-search region, bounded by the thick red box. These are all located near the upper boundary, between $\simeq$5–15 keVee.

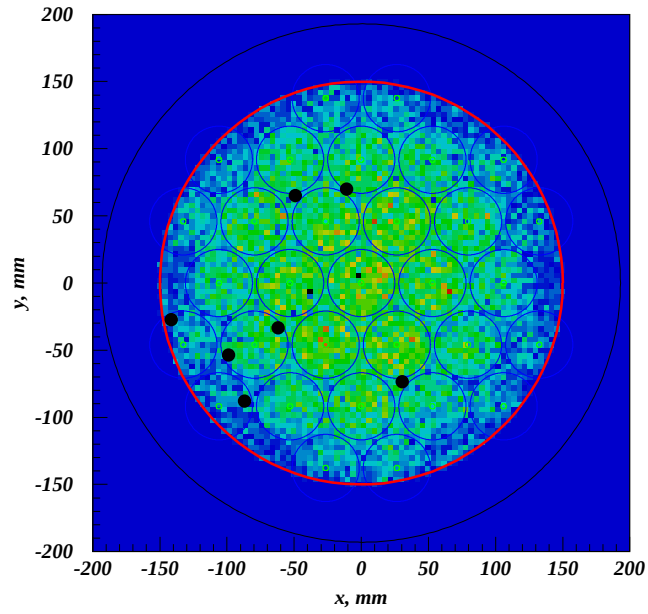

FIG. 13: Horizontal distribution of events in the energy range 2-16 keVee for the science run dataset. The reconstructed location of the 7 events in the acceptance region is indicated. This plot confirms the photomultipliers as the dominant source of γ-ray background.

1. *Efficiency and threshold*

In general the overall detection efficiency will be a combination of hardware and software effects. As mentioned earlier the hardware trigger threshold is derived from S2 for the low-energy part of the spectrum relevant to WIMP signals. Software effects include thresholding associated with pulse finding algorithms and selection cuts. Dead-time effects are usually energy independent. At higher energies, well beyond the upper limit of the WIMP search box, there is a high-level inhibit to suppress the overall count rate. A reasonable way of deriving efficiencies is to compare the differential spectrum seen during the nuclear-recoil calibration with a Monte Carlo simulation. Simulations done using GEANT4 are very well established for simple elastic scattering of neutrons and were extensively validated as part of this work. This comparison is shown in Figure 14. The energy scale associated with the simulated data have been converted from keVnr to keVee in Figure 14 by simply dividing by 2.09, to allow for the combination the relative nuclear-recoil scintillation efficiency to that of a 122 keV γ-ray at zero electric field, L_{eff}, and a suppression factor, S, which allows for the field-dependent variation in the scintillation output. These are used in the following equation:

$$E_{nr} = \frac{S1}{L_y}\frac{S_e}{L_{eff}S_n}\,, \qquad (1)$$

where S_e and S_n are the suppression factors in the scintillation output for 122 keV γ-rays and nuclear recoils, respectively, at the experiment operating fields. Note that in this equation the ratio $S1/L_y$ defines the keVee unit. Above $E_{nr}\sim$20 keV the available experimental data for L_{eff} suggests it is constant at ~ 0.19 [17, 18, 19].

By comparing the solid-line 'Simulation' curve with the 'Am-Be calibration data' histogram it can be seen that there is a very significant mismatch which builds up below $\sim$20 keVee. This mismatch far exceeds that expected from known efficiency and threshold effects as tabulated in Table I. The entries in the table have been checked using a number of independent methods and it is clear that they can only account for a small part of the discrepancy. All percentages are for events within the fiducial volume.

As a check on the energy dependence near the threshold a second AmBe dataset was analysed. These data had been acquired with a lower hardware trigger threshold. In addition, the 3-fold S1 coincidence requirement was changed to 2-fold in the analysis and all quality cuts removed or significantly relaxed. The resulting spectrum is shown in Figure 14 by the black histogram. This confirms that the difference is only noticeable below $\sim$5 keVee. In addition, a study of the smallest S2 events to trigger the system has shown directly that the trigger level in the two runs was $\sim$11 and $\sim$4 ionisation electrons, respectively. These numbers were calibrated against the measured single electron spectrum for ZEPLIN-III following the method already used for ZEPLIN-II [20]. Figure 15 shows the relative efficiency defined as the ratio of the

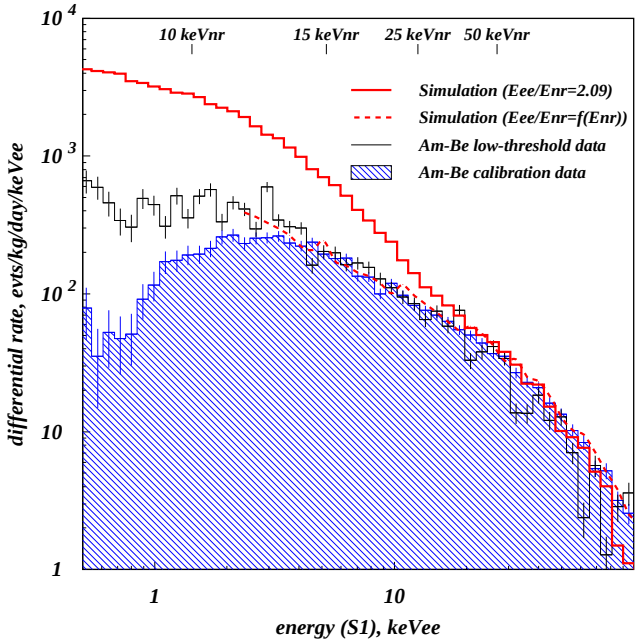

FIG. 14: Differential energy spectra for the AmBe elastic recoil population in S1 electron-equivalent units (^{57}Co-calibrated S1). The main calibration data (shaded blue histogram) and the lower threshold dataset described in the text (black) are compared with the Monte Carlo simulation using a constant conversion factor between nuclear recoil and electron equivalent energies (solid red curve). The ratio between these curves has often been interpreted as an energy-dependent efficiency factor. The dashed red curve is the result of the non-linearity analysis described in the text, which results in the energy conversion indicated by the markers at the top of the figure.

spectra in the blue and black histograms. In the following it is assumed that this curve correctly represents the energy-dependent part of the detection efficiency over the energy range of interest for WIMP searches. This means there must be another cause for the remaining mismatch between AmBe simulation and data. One possibility would be if there were some non-linearity in the energy conversion between keVee and keVnr and the next section looks at the requirements and consequences of this.

2. *Energy conversion*

In general the conversion between an electron-equivalent energy scale, in keVee, and a nuclear recoil energy scale, in keVnr, is not necessarily linear and any non-linearity could be expressed mathematically through energy dependency in L_{eff} and/or S_e/S_n. Above E_{nr}~20 keV the available experimental data for L_{eff} suggests it is constant at ~0.19. At lower energies the situation is much less clear [12]. For S_n there are no data on

TABLE I: Energy-independent efficiency factors and thresholds due to hardware and software actions. Efficiency figures are constant over the WIMP recoil range. Numbers following the entries refer back to the list of software operations itemised in Section III B. The total effective exposure is 126.7 kg·days.

Effect	**Efficiency**	**Method**
Deadtime	91.7%	Measured
Hardware upper threshold	100%	On-off compare
ZE3RA pulse finding (1)	96.0%	Timeline inspection
		Manual computation
Event reconstruction (2,3)	91.9%	Timeline inspection
Selection cuts (5)	73.0%	On-off compare
WIMP box acceptance	47.7%	
Effect	**Threshold**	**Method**
Hardware (S2) trigger	<1 keVee[a]	Two datasets
		Timeline inspection
		Modeling
		Pulser measurements
Software S2 area	<1 keVee	Calculation
		Scatter plots
Software S1 3-fold	1.7 keVee	Calculation
		Scatter plots

[a]The equivalent nuclear recoil energy, keVnr, depends on the conversion between keVee and keVnr. For the relationship shown in Section III D 2, 11 ionisation electrons corresponds to < 7keVnr

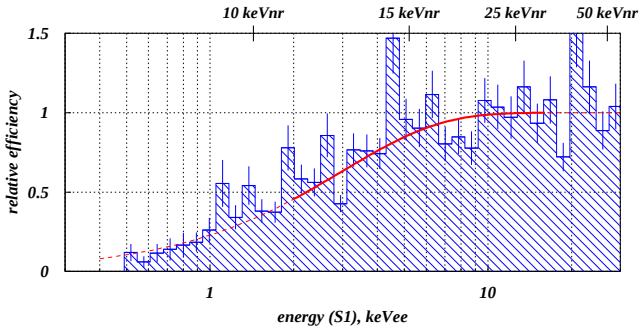

FIG. 15: Energy-dependent part of the nuclear recoil detection efficiency as deduced by comparing the two experimental AmBe spectra shown in Fig. 14. The 'low-threshold' run was taken with a lower hardware trigger threshold; in addition, software quality cuts were relaxed, along with the S1 3-fold requirement (to 2-fold). The fit to the data is shown, with the WIMP acceptance box indicated by the thicker portion of the line. We believe that the 'low-threshold' dataset has near-unity efficiency in the latter region.

the energy dependence but rather there is a single value based on a measurement at 56 keVnr using a neutron beam [18]. This gives $S_n = 0.90$ at our field and it is commonly assumed to then be constant over the whole energy range of WIMP nuclear recoils. If L_{eff} and/or S_n are not constant below ~20 keVnr this will cause a non-

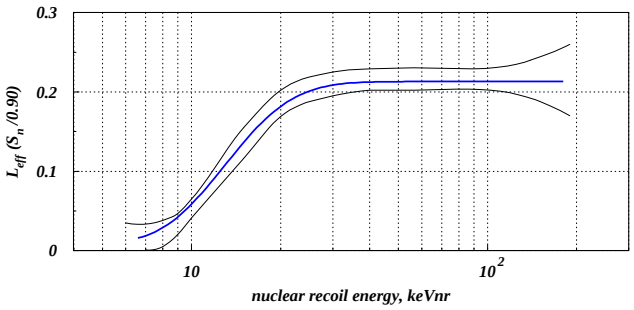

FIG. 16: The derived energy-dependent behaviour of $L_{eff}{\cdot}S_n$. The thick curve shows the best fit to the data, but other curves producing very similar goodness-of-fit indicators are obtained within the envelope shown. The constraints become very weak outside the energy range shown.

linearity in the nuclear recoil energy scale. In the following it is assumed that such non-linearities are responsible for the mismatch seen in Figure 14. The approach used is similar to that applied to the XENON10 data [12]. Using a maximum-likelihood technique we have derived a non-linearity function which best matches the AmBe simulation to our neutron calibration spectrum above ∼2 keVee. The outcome of this process is shown as the dashed red curve in Figure 14. Figure 16 expresses the nonlinearity in terms of the combined effect of L_{eff} and S_n. In Figures 14 and 15 the top horizontal axes show the energy scale in keVnr to be compared with keVee on the bottom scale. The WIMP search box boundaries then translate to 10.7 and 30.2 keVnr. One consequence of the required non-linearity is a marked reduction in efficiency for nuclear recoil detection below 15 keVnr.

3. *Maximum likelihood analysis*

The event box contains a large empty region with a small number of events close to where a tail from the electron recoil distribution would be expected. An appropriate method [21] for estimating the most probable WIMP signal is a two-parameter, binned maximum likelihood fit, with one parameter describing the signal population, S, and the other parameter, B, fitting the background tail from the electron recoil population. The fitting of the background distribution was carried out as described previously, independently in each of 14 1 keVee energy slices (2-16 keVee), by using a skew-Gaussian function over the entire S2/S1 parameter. This avoids biases by potential contamination from a small nuclear recoil signal. As noted earlier, the prediction for this background is 11.6±3.0 events, which is somewhat higher than the observation of 7 events in the box. In order not to over-constrain a possible signal component, the width of the electron-recoil distribution was allowed to vary within its own very small error range (whilst keeping the same overall integral) during the maximum likelihood fit. The signal population is the theoretical WIMP spectrum [22] derived using the standard spherical isothermal Galactic halo model (ρ_{dm}=0.3 GeVcm^{-3}, v_o=220 km/s, v_{esc}=600 km/s and v_{Earth}=232 km/s) detector response efficiencies and energy resolution. The form factor is taken from [23]. Both signal and background are characterised as a function of $\log_{10}(S2/S1)$ and energy, thus utilising as much information as possible about the observed event distribution.

Taking into account the expected WIMP energy spectrum, the overall maximum likelihood, $\mathcal{L}_{max}$, occurs for S=0, so the data are consistent with zero signal. The 90% upper signal limit is obtained by adding hypothetical signal levels and performing Monte Carlo simulations of a large number of such 'experiments', to give a likelihood distribution for each signal level [21]. The value of S for which only 10% of events in the likelihood distribution are compatible with $\mathcal{L}_{max}$ is the 90% upper confidence limit for S. We obtain S=2.9 events (for a WIMP mass of 55 GeV/c^2) for our data; this compares with S=2.3 for the Poisson upper limit for a box containing no events. The analysis must be repeated for different WIMP masses, with the limit varying from 2.45 events for a 10 GeV/c^2 WIMP to 3.0 events for a 1000 GeV/c^2 WIMP. The final result for the corresponding WIMP-nucleon spin-independent cross-section, shown in Figure 17, has a minimum in the 90% upper limit of $7.7{\times}10^{-8}$ pb for a WIMP mass of 55 GeV/c^2. In the mass range beyond 100 GeVc^{-2} this result complements the XENON10 result and further constrains the favoured SUSY parameter space [24] from xenon-based experiments. Spin-dependent limits will be presented separately and they will benefit slightly from an enhanced abundance of the non-zero spin isotopes in the xenon used in ZEPLIN-III.

IV. CONCLUSIONS

An analysis of 847 kg·days of data from the first science run of ZEPLIN-III has resulted in a signal lower limit consistent with zero, and an upper limit on the spin-independent WIMP-nucleon elastic scattering cross-section of $7.7{\times}10^{-8}$ pb, at 90% confidence level. In reaching this result it was necessary to confront an unexpected mismatch between the nuclear recoil spectrum shown in the AmBe calibration data and the Monte Carlo simulation. A careful and thorough analysis of efficiency factors and threshold effects (including the use of alternative datasets with different thresholds, systematic changes to software cuts and thresholds, visual scanning and manual analysis of large samples of data and modelling and direct verification of the performance of the DAQ) did not resolve this mismatch. As a more credible alternative explanation the possibility of a non-linearity in the nuclear recoil energy scale has been studied. Non-linearity as such is not unexpected and, indeed it would be surprising if it did not exist at low energy, and a similar

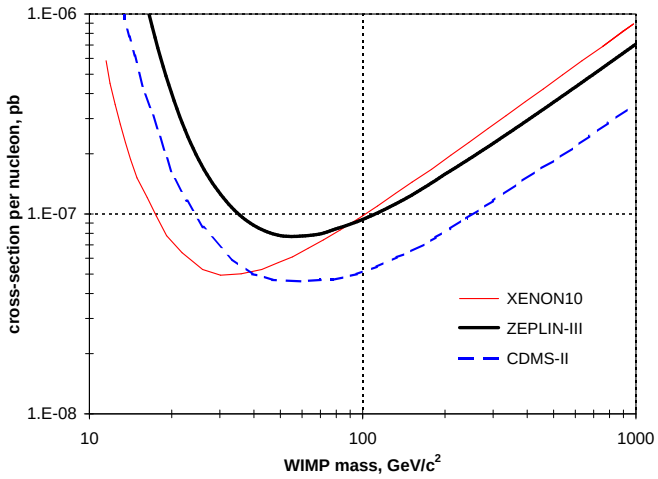

FIG. 17: 90% confidence upper limit to the WIMP-nucleon elastic scattering cross-section as derived from the first science run of ZEPLIN-III for a spin-independent interaction. For comparison, the experimental results from XENON10 [10, 25] and CDMS-II [26] are also shown. Note that the XENON10 curve is a 1-sided limit, corresponding approximately to an 85% confidence 2-sided limit [10]. CDMS-II and our result are both 90% 2-sided limits.

approach has been used by others for xenon [12]. Using this analysis it has been possible to reconcile the data with a non-linearity setting in at the same energy as in [12] but with a more significant trend to lower energies. In itself this again should not be surprising given the very different operating conditions within ZEPLIN-III and XENON10: the most obvious being that the electric field in the liquid is 6 times stronger. Indeed, there are other clear differences in the performances of the two instruments. However, it is clear that the physics underlying the low-energy performance is poorly understood. This is true of both the response to electron recoils [11] and to nuclear recoils [12]. As a point of reference, if the mismatch between the AmBe simulation and the data were interpreted solely as an instrument efficiency, the effect on the upper limit would not have been dramatic (<40% increase) as this approach has a better effective threshold for nuclear recoils but a poorer efficiency.

The analysis presented is not blind as one of the analysis routines was changed after opening of the full dataset. This was following the development of a significant improvement in the algorithms designed to identify MSSI events. The improvement had little effect on the nuclear recoil acceptance and the WIMP-search box definition was unchanged throughout.

Acknowledgements

The UK groups acknowledge the support of the Science & Technology Facilities Council (STFC) for the ZEPLIN-III project and for maintenance and operation of the underground Palmer laboratory which is hosted by the Cleveland Potash Ltd (CPL) at Boulby Mine, near Whitby on the North-East coast of England. The project would not be possible without the cooperation of the management and staff of CPL. We also acknowledge support from a Joint International Project award, held at ITEP and ICL, from the Russian Foundation of Basic Research (08-02-91851 KO a) and the Royal Society. We are indebted to our colleagues at ITEP, D.Yu Akimov, V. Belov, A. Burenkov and A. Kobyakin for their contributions. LIP-Coimbra acknowledges financial support from Fundação para a Ciência e Tecnologia (FCT) through the project-grants POCI/FP/81928/2007 and CERN/FP/83501/2008, the postdoctoral grant SFRH/BPD/27054/2006, as well as the PhD grants SFRH/BD/12843/2003 and SFRH/BD/19036/2004. The University of Edinburgh is a charitable body, registered in Scotland, with the registration number SC005336.

[1] G.J. Alner *et al.*, Astropart. Phys. **23**, 444 (2005)
[2] G.J. Alner *et al.*, Astropart. Phys. **28**, 287 (2007)
[3] H.M. Araújo *et al.*, Astropart. Phys. **26**, 140 (2006)
[4] D.Yu. Akimov *et al.*, Astropart. Phys. **27**, 46 (2007)
[5] H.M. Araújo *et al.*, Nucl. Instrum. Meths. A **521**, 407 (2004)
[6] B.A. Dolgoshein, V.N. Lebedenko, B.U. Rodionov, JETP Lett.**11** 513 (1970)
[7] V.N. Solovov *et al.*, In preparation (2008)
[8] A. Lindote *et al.*, Nucl. Instrum. Meths. A **573**, 200 (2007)
[9] F. Neves *et al.* In preparation (2008)
[10] J. Angle *et al.*, Phys. Rev. Lett. **100**, 021303 (2008)
[11] T. Shutt *et al.*, Nucl. Phys. B Proc. Suppl. **173**, 160 (2007)
[12] P. Sorensen *et al.*, arXiv:0807.0459S (2008)
[13] http://wwwasdoc.web.cern.ch/wwwasdoc/hbook_html3/hboomain.html
[14] http://wwwasd.web.cern.ch/wwwasd/paw/
[15] http://root.cern.ch/
[16] S. Agostinelli *et al.*, Nucl. Instrum. Meths. A **506**, 250 (2003)
[17] D. Akimov *et al.*, Phys. Letts. B **524**, 245 (2002)
[18] E. Aprile *el al.*, Phys, Rev. D **72**, 072006 (2005)
[19] V. Chepel *el al.*, Astropart. Phys. **26**, 58 (2006)
[20] B. Edwards *et al.*, Astropart. Phys. **30**, 54 (2008)
[21] G Cowan, Statistical Data Analysis, Oxford University Press, ISBN 0198501552 (1998)
[22] J.D. Lewin, P.F. Smith, Astropart. Phys. **6**, 87 (1996)
[23] R.H. Helm, Phys. Rev. **104**, 1466 (1956)
[24] L. Roszkowski, R. Ruiz de Austri, and R. Trotta, J. High Energy Phys. **07**, 075 (2007)
[25] E. Aprile *el al.*, arXiv:0810.0274 (2008)
[26] Z. Ahmed *et al.*, arXiv:0802.3530v2 (2008)